J. Geogr. Sci. 2022, 32(2): 241-258
DOI: https://doi.org/10.1007/s11442-022-1945-1

How is the precipitation distributed vertically in arid mountain region of Northwest China?

YANG Yanfen, SHEN Lulu, *WANG Bing

State Key Laboratory of Soil Erosion and Dryland Farming on the Loess Plateau, Institute of Soil and Water Conservation, Northwest A&F University, Yangling 712100, Shaanxi, China

Abstract: Precipitation in the arid region of Northwest China (NWC) shows high spatial and temporal variability, in large part because of the region's complex topography and moisture conditions. However, rain gauges in the area are sparse, and most are located at altitudes below 2000 m, which limits our understanding of precipitation at higher altitudes. Interpolated precipitation products and satellite-based datasets with high spatiotemporal resolution can potentially be a substitute for rain gauge data. In this study, the spatial and temporal properties of precipitation in the arid region of NWC were analyzed using two gridded precipitation products: SURF_CLI_CHN_PRE_DAY_GRID_0.5 (CHN) and Tropical Rainfall Measuring Mission (TRMM) 3B43. The CHN and TRMM 3B43 data showed that in summer, precipitation was more concentrated in southern Xinjiang than in northern Xinjiang, and the opposite was true in winter. The largest difference in precipitation between mountainous areas and plains appeared in summer. High-elevation areas with high precipitation showed more stable annual precipitation. Different sub-regions showed distinctive precipitation distributions with elevation, and both datasets showed that the maximum precipitation zone appeared at high altitude.

Keywords: gridded precipitation; mountainous areas; temporal variability; altitudinal distribution

1 Introduction

The arid region of Northwest China (NWC) is located at the innermost center (34°–50°N, 72°–107°E) of the Eurasian continent. Because this area is far from any ocean, it experiences water shortages and a generally dry climate (Shi *et al*., 2007). The high mountains in this area play an important role in capturing and lifting vapor, and also in increasing the mountainous precipitation. Water resources in Xinjiang (which covers almost 78% of the arid region of NWC) originate mainly from precipitation in high-altitude mountainous areas. Precipitation in mountainous areas reportedly accounts for 84.3% of the total annual precipitation (Zhang and Zhang, 2006) and makes an important contribution to runoff formation.

In recent years, the spatial and temporal characteristics of precipitation in the arid region of NWC have been studied. Overall, precipitation in this area exhibits an apparent nonlinear

Received: 2021-05-14 **Accepted:** 2021-10-20
Foundation: National Natural Science Foundation of China, No.42130717
Author: Yang Yanfen (1984–), Assistant Professor, specialized in hydrological process. E-mail: yfyang@ms.iswc.ac.cn
*Corresponding author: Wang Bing (1982–), Professor, E-mail: bwang@ms.iswc.ac.cn

upward trend and shows notable spatial differences; northern Xinjiang exhibits mainly an upward trend, whereas southern Xinjiang shows mainly increasing or decreasing–increasing trends. The precipitation variation in the Hexi Corridor is more complex (Qin *et al*., 2018). Wang *et al*. (2020) and Hu *et al*. (2021) also found that annual precipitation and extreme precipitation in Xinjiang have increased since 1985, mainly in the northern and western mountains of Xinjiang. The average increase rate of precipitation from 1960 to 2016 was 5.82 mm/10a in the Tianshan Mountains, and the highest and lowest increase rates were 9.22 mm/10a at 1500–2000 m and 3.45 mm/10a at 500 m, respectively (Xu *et al*., 2018). Chen *et al*. (2018) found that on the northern side of the Qilian Mountains, the maximum precipitation height was approximately 2300 m in winter and approximately 4200 m in other seasons. However, most previous studies have focused on the spatiotemporal variation of precipitation in the arid region of NWC, whereas studies of the vertical precipitation distribution have been limited by sparse gauge observation data for high-altitude areas.

Vertical precipitation profiles are very important for hydrological research in mountainous areas (Pratap *et al*., 1995; Barros *et al*., 2006). Precipitation–elevation relationships are usually derived from precipitation data at different elevations (Li *et al*., 2009; Chen, 2010; Zhao *et al*., 2011). However, it can be difficult to derive these relationships for high-elevation zones where measurements are often unavailable. Efforts have been made to derive the precipitation–elevation relationships for the high mountains of NWC, but the results often have high uncertainty. For example, in the central part of northern slope of the Tianshan Mountains, data collected between June and August, 1956, showed two precipitation maxima along the elevation profile, at 1850 and 3539 m, respectively (Shen and Liang, 2004; Li, 2006; Zhao *et al*., 2011). However, Lauscher (1976) concluded that only one precipitation maximum existed in this area. Ultimately, these differences occur because we do not have sufficient data regarding precipitation at high elevations.

Precipitation is conventionally measured by rain gauges, which are considered to be the most accurate method of near-surface precipitation measurement (Xie and Arkin, 1995), although they suffer from unavoidable errors such as wind loss, splashing, and evaporation (Legates and DeLiberty, 1993). The number of rain gauges in the arid region of NWC is very limited, and the gauges are not uniformly distributed, as shown in Figure 1. On average, one rain gauge covers an area of 28,000 km^2, and more than 90% of the gauges are located below 2000 m above sea level (asl). Thus, precipitation data above 2000 m asl are extremely scarce. In addition, because of the complex local topography and atmospheric moisture conditions, precipitation in this area shows strong spatial and temporal variability. As a result, the representative scope of rain gauge data is limited (Collischonn *et al*., 2008), resulting in unrepresentative observations over large regions (Groisman and Legates, 1994; Sinclair *et al*., 1997; Boushaki *et al*., 2009).

The lack of precipitation measurements in high mountainous areas is a common problem, and thus precipitation products based on remote sensing, such as Precipitation Estimation from Remotely Sensed Information using Artificial Neural Networks (PERSIANN) (Hsu *et al*., 1997), the Climate Prediction Center's morphing technique (CMORPH) (Joyce *et al*., 2004), and Tropical Rainfall Measuring Mission (TRMM) (Huffman *et al*., 2007), are increasingly used as alternative data worldwide. In addition, gridded datasets based on interpolation from rain gauges, such as SURF_CLI_CHN_PRE_DAY_GRID_0.5 (CHN), are

valuable sources of precipitation data in mountainous areas. These remote sensing-image based products and ground data based interpolated datasets feature high spatiotemporal resolution and continuous coverage even in high-elevation areas, which are crucial to hydrometeorological studies.

Thus, this study focuses on the horizontal spatial distribution patterns of precipitation in the arid region of NWC as revealed by different gridded data sources and analyzing the vertical precipitation distribution with altitude by adopting gridded precipitation data sources. These efforts may provide a general understanding of the precipitation distributions over this region.

2 Data and methodology

2.1 Study area

The arid region of NWC (Figure 1), including the entire Xinjiang Uygur Autonomous Region, the Hexi Corridor in Gansu Province, the western Helan Mountains in the Inner Mongolia Autonomous Region, and parts of Qinghai Province and the Ningxia Hui Autonomous Region, covers an area of 2.27 million km^2 (Chen, 2010; Zhang *et al*., 2011; Qin *et al*., 2018). The topography of this region is very complex. The defining morphological features of the entire region are mountains, which generally run east to west, with interspersed basins. The Tianshan Mountains extend across the center of Xinjiang and divide it into two regions, commonly known as southern Xinjiang and northern Xinjiang (Chen *et al*., 2012; Zhang *et al*., 2012). The Altay Mountains extend along the northern edge of the study area, and the Karakoram Mountains run along its southern edge. Between the Altay and Tianshan Mountains lies the Junggar Basin, whereas the Tarim Basin lies between the Tianshan and Kunlun Mountains. The elevation of this region ranges from −154.31 m asl (Aydingkol Lake) to 8611 m asl (Mount Qogir), as reported by the National Bureau of Surveying, Mapping, and Geoinformation of the People's Republic of China; 16.4% of the study area is located above 3510 m asl, where rain gauges are rarely installed. According to Chen (2010), the elevation demarcation points between mountainous areas and plains are 1000 m for the Altay Mountains and the northern slope of the Tianshan Mountains, 1500 m for the Qilian Mountains and the southern slope of the Tianshan Mountains, and 2000 m for the Kunlun Mountains (Figure 1).

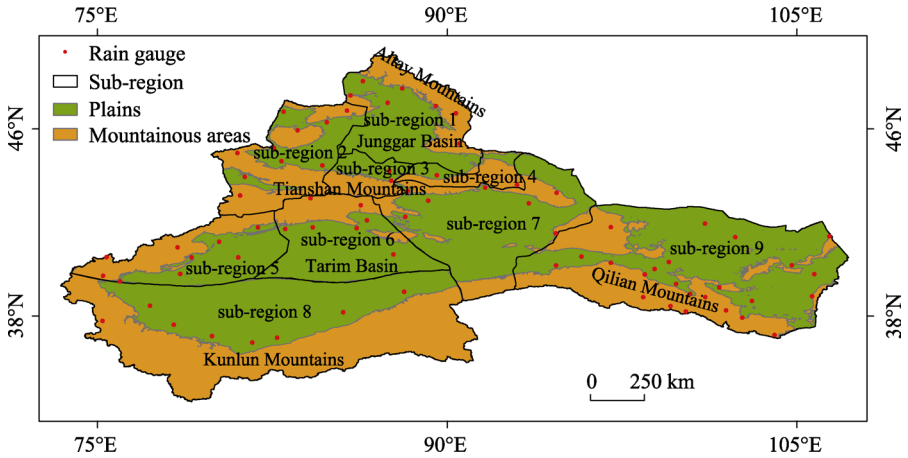

Figure 1 Location and rain gauges of arid mountain region of Northwest China

The study area has a broad scope, and its climate, topography, and land cover are all complex. To enable better description of relevant spatial patterns, this area was divided into nine sub-regions reflecting the impact of topography on the local climate, following Mu (2010) and Zhao (2011), as shown in Figure 1 and Table 1. The regionalization was based on the relationship between elevation and precipitation from rain gauge data according to Zhao (2011). The precipitation is highly correlated with elevation in each sub-region. The choice of divisions was informed primarily by the presence of mountains, the slope aspect of the mountains, and the further division of the Tianshan Mountains into three sections (the western, central, and eastern portions). The nine sub-regions are numbered sequentially from north to south and from west to east. For example, sub-region 1 consists mainly of the southern slope of the Altay Mountains and the northern part of the Junggar Basin, which are located in northern Xinjiang. The Tianshan Mountains are divided into the northern slope (windward slope) and southern slope (leeward slope). Sub-regions 2, 3, and 4 contain the western, central, and eastern portions of the northern slope of the Tianshan Mountains, and sub-regions 5, 6, and 7 contain the western, central, and eastern portions of the southern slope of the Tianshan Mountains. Sub-region 8 is the northern slopes of the Karakoram and Kunlun mountains and the southern Tarim Basin. Sub-region 9 is the northern slope of the Qilian Mountains. The areas of these sub-regions range from 4.5×10^4 km^2 to 6.7×10^5 km^2, of which mountainous areas account for 22%–68.4%. Precipitation–elevation profiles were derived to show relevant vertical distribution patterns, which are discussed with respect to each region.

Table 1 Geographic and physical characteristics of sub-regions in arid mountain region of Northwest China

Sub-regions		Area (km^2)		Elevation (m)			Scope
No.	Name	Total	Mountains	Max	Min	Mean	
1	Southern slope of Altay Mountains	173,000	59,400	4354	187	1001	44.0°–49.0°N 85.0°–91.1°E
2	Western part of northern Tianshan Mountains	171,000	102,000	6323	107	1489	42.5°–47.3°N 80.1°–86.6°E
3	Central part of northern Tianshan Mountains	48,500	24,500	5251	197	1521	43.0°–45.2°N 84.6°–88.6°E
4	Eastern part of northern Tianshan Mountains	45,000	30,800	4325	369	1361	43.4°–45.2°N 87.7°–93.4°E
5	Western part of southern Tianshan Mountains	179,000	777,000	7406	895	1829	39.6°–42.4°N 73.8°–83.3°E
6	Central part of southern Tianshan Mountains	193,000	46,900	4808	654	1377	39.9°–43.3°N 81.6°–90.2°E
7	Eastern part of southern Tianshan Mountains	284,000	62,600	5049	154.31	1222	38.6°–45.0°N 86.8°–96.4°E
8	Northern slope of Karakoram and Kunlun mountains	672,000	365,000	8611	637	2917	35.9°–40.0°N 73.4°–91.4°E
9	Northern slope of Qilian Mountains	502,000	199,000	5840	659	1702	36.9°–42.1°N 92.8°–107.3°E

2.2 Datasets

The remote-sensing-based precipitation products mentioned above [TRMM 3B42, TRMM 3B43 (Huffman *et al*., 2010), CMORPH, and PERSIANN] were evaluated in our previous work (Yang and Luo, 2014a). The results showed that TRMM 3B43 performed best, whereas CMORPH and PERSIANN overestimated the precipitation to a greater extent. A back-propagation neural network approach was later proposed and used to correct the bias of

TRMM 3B43, and acceptable biases and accuracy were obtained (Yang and Luo, 2014b). Thus, the bias-corrected version of TRMM 3B43 was used in this study. The data have a spatial resolution of 0.25° and a temporal resolution of one month; they cover January 1998 to December 2010.

In addition, CHN, a gridded daily precipitation dataset based on interpolation from rain gauge data that covers only China, was also used in this study. CHN is open-source and is published by the China Meteorological Data Service Centre (http://http://data.cma.cn/). It is generated by thin-plate spline interpolation of data from 2474 rain gauges spanning 1961 to the present. The spatial resolution is 0.5°. This dataset has good quality, as demonstrated by cross-validation and error analysis. CHN was resampled to a spatial resolution of 0.25° using ArcGIS software before the analysis so that it has the same resolution as TRMM 3B43. According to Yang and Luo (2014b), who analyzed the representative range of precipitation and topography in detail, a 0.25° grid is sufficient to represent the complexity of the terrain.

The Advanced Spaceborne Thermal Emission and Reflection Radiometer digital elevation model (DEM) data, with coverage from 83°N to 83°S and a resolution of 1 arcsec (30 m horizontal spacing at the equator), were used to extract an elevation value for each grid cell. These data are available via the National Aeronautics and Space Administration Warehouse Inventory Search Tool.

2.3 Analysis of precipitation patterns

The spatial and temporal distribution patterns of precipitation in the arid region of NWC are the main topic of this study. On the temporal scale, TRMM 3B43 and CHN data were used to analyze the variability of seasonal precipitation and the interannual variation in the mountainous areas, plains, and each of the nine sub-regions. For the horizontal dimension, precipitation contour maps based on these two precipitation products were drawn and analyzed. For each sub-region, the areal precipitation was calculated and compared to previous studies. The precipitation concentration index (PCI) was used to represent the concentration degree of precipitation. It was proposed by Oliver (1980) and developed by De Luis *et al*. (1997). The PCI has a more intuitive physical meaning and simpler calculation than other indices (Zhang *et al*., 2021). The seasonal time scale is defined as follows:

$$PCI = \frac{\sum_{i=1}^{3} P_i^2}{\left(\sum_{i=1}^{3} P_i\right)^2} \times 25 \tag{1}$$

where P_i is the monthly precipitation in the ith month for each gauge or grid. *PCI* values of less than 10 indicate a uniform precipitation distribution (low precipitation concentration), and values between 10 and 15 indicate moderate precipitation concentration. Values between 15 and 20 represent an irregular precipitation distribution, and values above 20 represent strong irregularity in the precipitation distribution.

The distribution of precipitation in each sub-region across the vertical profiles was calculated. The precipitation for each grid cell was represented separately by the means of the TRMM 3B43 and CHN data for that cell, and the mean value for the corresponding grid cell from the DEM data was extracted to represent elevation. This enabled one-to-one matching

of precipitation and elevation for each dataset. Next, the precipitation and elevation were averaged in each 300 m elevation band for each sub-region, which allowed us to construct a set of vertical profiles for each dataset. The confidence bands (CBs) of the two datasets were both determined by Equation (2) at the 95% confidence level.

$$CB = \overline{X} \pm 1.96\left(\frac{\delta}{\sqrt{n}}\right) \tag{2}$$

where CB is bounds of the confidence band, $\overline{X}$ is the average value of the dataset, δ is the standard deviation, and n is the sample size. The precipitation–elevation profiles generated by the two datasets were compared, and the distribution features in each sub-region are discussed with reference to other reports in the literature. Analysis over all three dimensions thus yields an overall picture of the spatial distribution patterns of precipitation in the arid region of NWC.

3 Result and discussion

3.1 Temporal variability of precipitation

The temporal variability of precipitation was analyzed in terms of seasonal distribution and interannual variation using both TRMM 3B43 and CHN data (separately) for mountainous areas, plains, and each of the nine sub-regions. Seasonal differences in precipitation were evident, as shown in Table 2.

Owing to the monsoon, the precipitation in NWC and its sub-regions was concentrated mainly in summer, which accounted for 36.4% to 69.8% of the average annual precipitation, whereas winter precipitation accounted for only 2.5% to 14%. The precipitation was more concentrated in summer in southern Xinjiang than in northern Xinjiang, accounting for 48.7%–69.8% and 36.4%–51.4% of the annual precipitation, respectively. In winter, however, the opposite trend appeared; the proportion of precipitation in southern Xinjiang was 2.8%–8.7%, whereas that in northern Xinjiang was 6%–14%.

Seasonal differences in precipitation also appeared between mountainous areas and plains because of differences in elevation, available moisture, and dynamic conditions. The most notable difference was that precipitation was higher in mountainous areas than in plains. The largest difference appeared in summer, where mountain areas received 57–204 mm of precipitation, whereas plains received much less (17–86 mm).

The interannual variation of precipitation can be characterized by variation coefficients, where larger values indicate more unstable annual precipitation, whereas smaller ones indicate little interannual variation in precipitation. Table 3 shows that the variation coefficients ranged from 0.08 to 0.19 for TRMM 3B43 and from 0.14 to 0.23 for CHN on the sub-region scale. The variation coefficients for mountainous areas were higher by 0.01–0.16 than those for plains for TRMM 3B43 and higher by 0.02–0.17 for CHN. This result indicates that the interannual variation of precipitation was smaller in mountainous areas than in plains. High-altitudes areas, which receive more precipitation, exhibited more interannual stability in precipitation.

3.2 Horizontal precipitation distribution

The precipitation in mountainous areas is reportedly several times, or even dozens of times,

Table 2 Seasonal precipitation in sub-regions, mountainous areas, and plains in arid mountain region of Northwest China

Region		Spring (%)	Summer (%)	Autumn (%)	Winter (%)	Sum (mm)	Spring (%)	Summer (%)	Autumn (%)	Winter (%)	Sum (mm)
		TRMM 3B43					CHN				
Sub-region	1	25.7	36.4	23.9	14.0	187	23.5	40.0	23.8	12.6	225
	2	25.9	42.6	21.9	9.6	354	25.6	48.9	18.6	6.9	334
	3	24.1	40.0	22.3	13.5	265	24.6	51.4	17.7	6.3	305
	4	22.6	44.9	21.3	11.1	192	23.9	49.5	20.6	6.0	216
	5	21.9	54.8	18.7	4.6	148	23.3	56.6	16.7	3.5	158
	6	13.3	68.6	12.6	5.5	99.8	14.9	69.3	13.0	2.8	101
	7	30.2	48.7	13.7	7.4	53.0	19.4	60.3	16.2	4.1	78.1
	8	20.1	54.4	16.9	8.7	110	14.5	69.8	11.9	3.9	89.3
	9	18.8	54.5	23.1	3.6	115	16.3	63.5	17.6	2.5	136
	NWC	21.2	51.6	19.1	8.1	137	20.0	57.2	17.3	5.5	143
Mountainous areas	1	25.9	37.9	23.7	12.5	285	22.2	41.0	23.2	13.7	306
	2	25.3	45.9	21.8	7.1	445	24.9	52.3	17.6	5.3	408
	3	27.9	38.2	20.4	13.4	315	21.9	58.9	15.2	4.0	396
	4	22.4	45.7	21.8	10.2	189	23.6	51.4	19.8	5.1	232
	5	20.6	55.3	20.4	3.6	246	24.5	55.7	16.9	2.9	274
	6	13.9	71.1	11.4	3.5	259	14.0	71.3	12.7	2.0	255
	7	21.4	62.3	11.3	4.9	90.9	20.9	59.4	16.0	3.7	165
	8	19.3	53.7	18.0	9.0	164	12.2	72.6	11.8	3.3	128
	9	17.6	58.3	21.5	2.6	178	16.6	64.2	16.7	2.5	211
	NWC	21.3	52.1	18.9	7.7	242	21.0	56.9	17.0	5.0	264
Plains	1	27.0	34.1	23.2	15.7	137	24.7	39.2	24.4	11.8	184
	2	24.3	35.9	23.8	16.0	218	27.5	39.7	21.3	11.5	223
	3	26.3	39.9	19.7	14.0	214	29.9	37.0	22.3	10.8	212
	4	24.6	44.2	17.9	13.3	195	24.7	44.3	22.7	8.3	183
	5	20.8	53.6	18.9	6.8	78.2	20.2	58.7	16.0	5.1	74.9
	6	16.7	61.6	12.4	9.3	45.9	16.6	65.7	13.5	4.2	48.3
	7	35.4	40.5	15.2	8.9	42.4	18.1	61.0	16.4	4.6	53.7
	8	23.0	54.1	13.4	9.5	48.0	21.7	60.5	11.9	5.9	45.0
	9	20.6	49.0	25.4	5.0	75.5	15.9	62.4	19.1	2.6	89.2
	NWC	20.9	53.9	18.5	6.7	117	24.5	46.0	20.7	8.9	124

greater than that in basins. Northern Xinjiang receives more precipitation than southern Xinjiang (Xie *et al*., 2017). In the Tianshan Mountains, the northern slope (windward side) receives more precipitation than the southern slope (leeward side), and the precipitation gradually decreases from west to east (Chen, 2010). The Ili Valley of the western Tianshan Mountains, which is affected by the westerly current and plentiful of water vapor, receives the most precipitation in the study area (Shi *et al*., 2008). The Altay Mountains are affected mainly by the Arctic current, which carries only one-third or one-fourth the water vapor of the westerly current; consequently, the Altay Mountains receive less precipitation than the Tianshan Mountains (Su *et al*., 2007). The eastern and western parts of the Qilian Mountains

Table 3 Interannual change (variation coefficient) of precipitation for sub-regions, mountainous areas, and plains in arid mountain region of Northwest China

Dataset	Sub-region No.	Sub-region	Mountainous areas	Plains
TRMM 3B43	1	0.12	0.1	0.14
	2	0.08	0.07	0.11
	3	0.14	0.12	0.17
	4	0.17	0.16	0.19
	5	0.19	0.16	0.28
	6	0.08	0.09	0.1
	7	0.12	0.12	0.14
	8	0.14	0.11	0.27
	9	0.15	0.11	0.22
CHN	1	0.21	0.24	0.22
	2	0.15	0.15	0.19
	3	0.15	0.14	0.21
	4	0.2	0.19	0.21
	5	0.23	0.22	0.33
	6	0.17	0.15	0.32
	7	0.19	0.17	0.21
	8	0.22	0.25	0.38
	9	0.14	0.13	0.21

are affected by the southeast monsoon and westerly current, respectively. Moisture is more plentiful in the eastern part than in the western part, and the eastern part thus receives more precipitation (Zhang *et al*., 2008; Chen, 2010). The Junggar and Tarim basins, however, which are located in the hinterland of the Eurasian continent and far from the ocean, receive the least precipitation (Zhang and Yuan, 2002; Li, 2003; Chen, 2010).

Judging visually from the contour maps of precipitation (Figure 2), the spatial precipitation distributions presented by CHN and TRMM 3B43 were consistent with the characteristics described above. The maps showed that precipitation was concentrated mainly in the mountainous areas, whereas the plains received much less precipitation than the mountains. Table 4 lists the annual precipitation estimated from the two grid datasets for each of the nine sub-regions for reference.

Table 4 Rough estimate of annual precipitation in arid mountain region of Northwest China

Sub-regions	Area (10^4 km^2)	Depth (mm)		Volume (10^9 m^3)	
		TRMM 3B43	CHN	TRMM 3B43	CHN
1	17.3	187	225	32.0	39.0
2	17.1	354	334	61.0	57.0
3	4.85	265	305	13.0	15.0
4	4.50	192	216	8.6	9.7
5	17.9	148	158	27.0	28.0
6	19.3	100	101	19.0	19.0
7	28.4	53.0	78.0	15.0	22.0
8	67.2	110	89.0	74.0	60.0
9	50.2	115	136	58.0	68.0

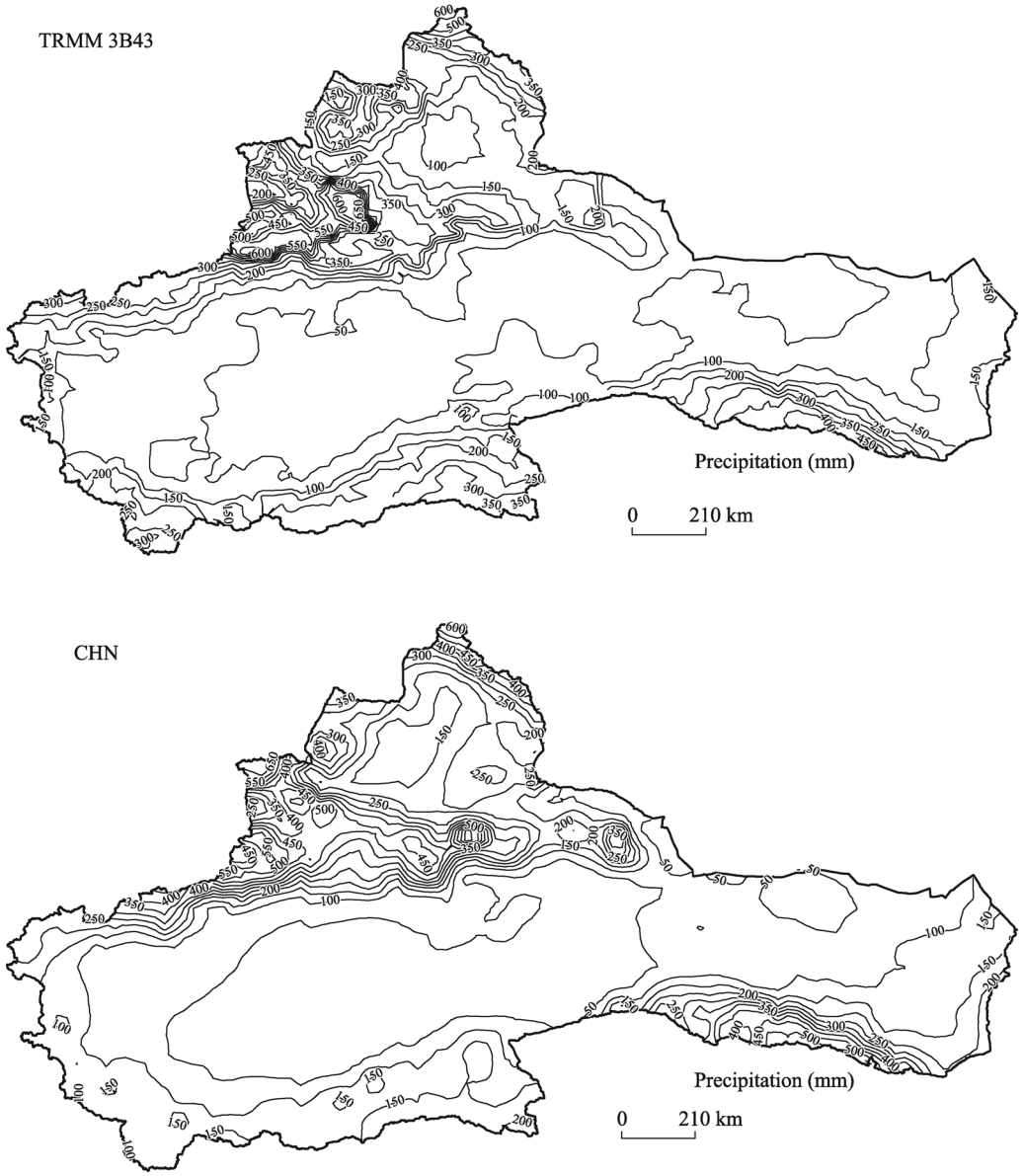

Figure 2 Contour maps of annual precipitation given by TRMM 3B43 and CHN in arid mountain region of Northwest China

Table 5 lists the estimated annual precipitation in different parts of the study area from the two datasets; literature values are also given for comparison. The latter were derived from rain gauge observations for each specific region using an arithmetic method. Comparison analysis may reveal the performance of the two grid datasets in different sections. Zhang *et al*. (2011) indicated that the annual precipitation over the entire study area is at most 200 mm, whereas Chen (2010) estimated it at 151 mm, and Guo *et al*. (2020) indicated that it is approximately 130 mm and decreases from east to west. TRMM 3B43 and CHN gave values of 137 and 143 mm, respectively, which were similar to the results of Chen (2010) and Guo *et al*. (2020). Northern and southern Xinjiang reportedly receive 254–278 mm and 116 mm,

respectively, of precipitation annually (Su *et al*., 2007; Chen, 2010). The TRMM 3B43 and CHN datasets gave estimations of 259 and 273 mm for northern Xinjiang, and 100 and 98 mm for southern Xinjiang, respectively. These estimates are reasonable for northern Xinjiang and slightly (16–18 mm) lower than the literature values for southern Xinjiang. In Gansu and Inner Mongolia, the annual precipitation estimates from TRMM 3B43 and CHN were 115 and 136 mm, respectively; these values are 15 mm lower and 6 mm higher than the value of 130 mm obtained by Chen (2010).

Table 5 Annual precipitation for each sub-region in arid mountain region of Northwest China with literature values for comparison

Region	TRMM 3B43 (mm)	CHN (mm)	Literature values (mm)
Entire study area	137	143	151
Northern Xinjiang (sub-regions 1–4)	259	273	254–278
Southern Xinjiang (sub-regions 5–8)	100	98	116
Gansu and Inner Mongolia (sub-region 9)	115	136	130

Note: The literature values are from Chen (2010) and Su *et al*. (2007).

The spatial distribution of the PCI in summer (Figure 3) showed values of 8.8–10.8 for the gauge data, 8.3–10.2 for the CHN data, and 8.3–11 for the TRMM data, respectively. The mean values were 8.3, 8.7, and 8.9 for the gauge, CHN, and TRMM data, respectively. The PCI from the TRMM data was slightly higher than those from the gauge and CHN data. On the spatial scale, the three datasets consistently indicated moderate precipitation concentration ($10 \leqslant \mathrm{PCI} < 15$) in a few areas of the northern slopes of the Karakoram and Kunlun mountains (sub-region 8), whereas the precipitation was uniformly distributed in the other sub-regions.

3.3 Altitudinal distributions of annual precipitation

The grid cells for each sub-region were grouped in elevation bands of 300 m, and the elevation in each range is given as the average value. In each elevation band, the grid cell precipitation was statistically analyzed. The average values with the CBs at P = 95% were then plotted against elevation, showing the precipitation distribution pattern in the vertical dimension for each sub-region (Figure 4).

The TRMM 3B43 and CHN data showed that precipitation generally increased with elevation, although it may begin to decrease at some elevations in some sub-regions. Quantitatively, however, the CHN dataset gave higher precipitation than TRMM 3B43 except in the western part of the northern slope of the Tianshan Mountains and the northern slopes of the Karakoram and Kunlun mountains (sub-regions 2 and 8).

The most complicated profile was found on the southern slope of the Altay Mountains (sub-region 1), where the precipitation began to decrease with elevation between approximately 2560 and 3100 m and then increased above 3100 m. Some previous studies have found that precipitation increased with elevation and decreased at approximately 2000 m asl (Zhang and Deng, 1987; Su *et al*., 2007). Ning *et al*. (2020) indicated that the first and second precipitation peaks appeared at approximately 2400 and 3200 m, respectively; these values are similar to our results.

For the northern slope of the Tianshan Mountains (sub-regions 2, 3, and 4), studies based on limited rain gauge data have indicated that the only maximum relative humidity layer

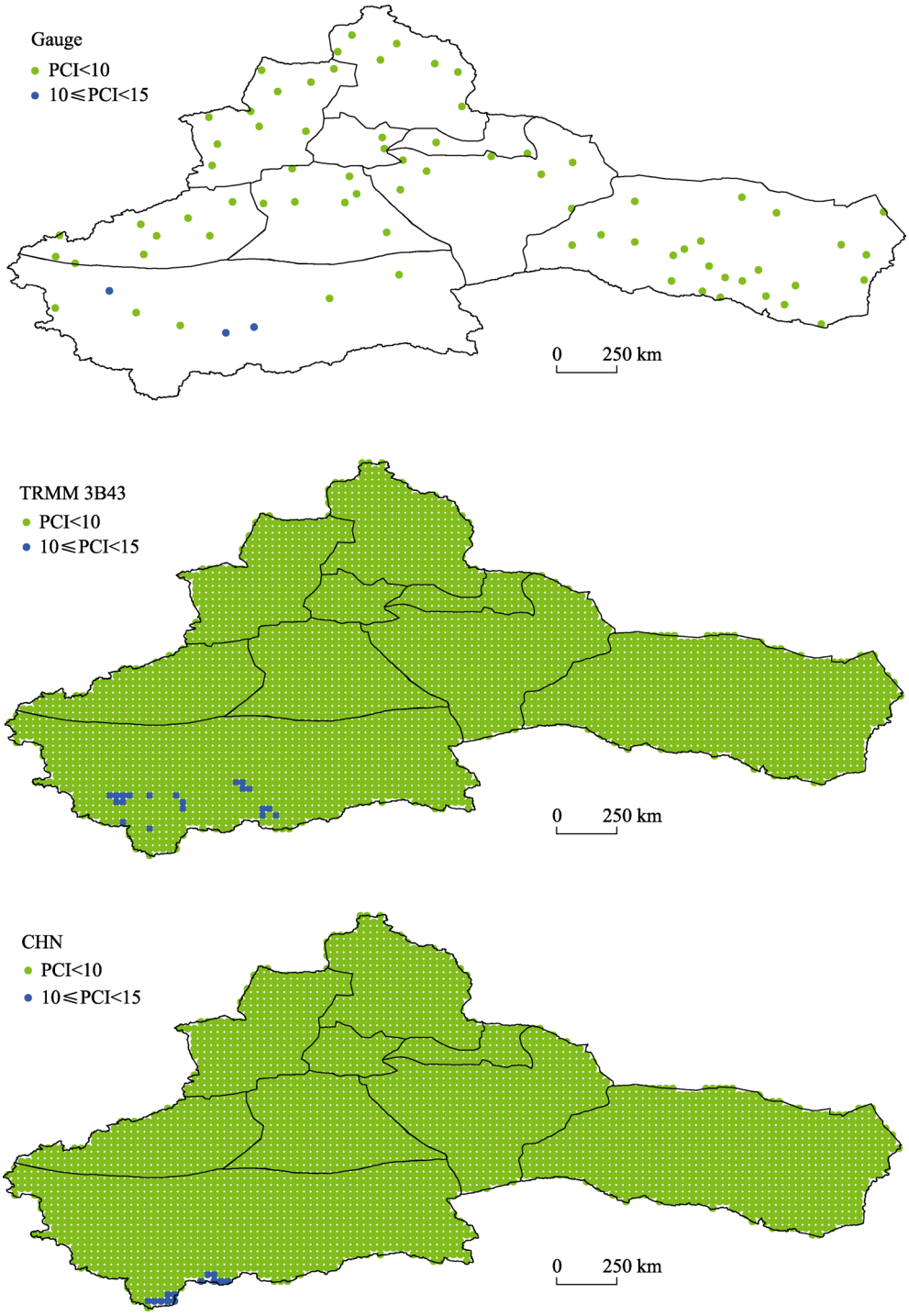

Figure 3 Spatial distribution of precipitation concentration index (PCI) in summer for gauge, TRMM 4B43 and CHN in arid mountain region of Northwest China

resulted in the unique zone of maximum precipitation (Zhang and Deng, 1987); however, the location of the zone varied, for example, 1600–2100 m asl by Lin (1995), 2000 m asl by Lin (1985), 2160 m asl by Zhang and Deng (1987), and 2400 m asl by Weng (1985), probably

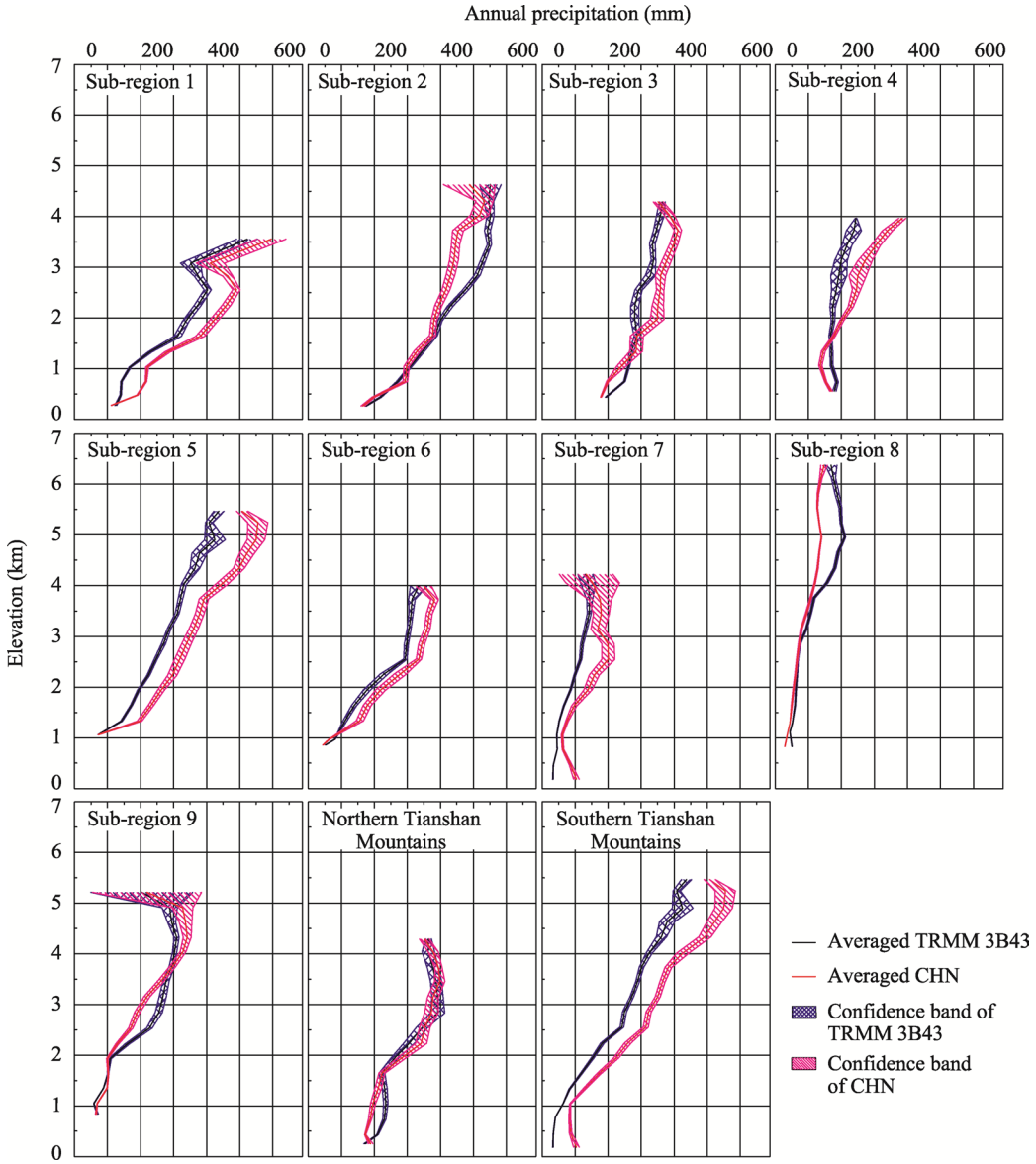

Figure 4 Altitudinal distribution patterns of annual precipitation in arid mountain region of Northwest China derived from different datasets with confidence bands at P = 95%

because of differences in data source. Some studies reported that there were two peaks in the precipitation profile in the northern Tianshan Mountains. The first peak is reportedly located at 1600–2000 m asl (Chen, 2010) or 2000 m asl (Su *et al*., 2007); the second reportedly lies at 3500 m (Su *et al*., 2007) or 4000 m (Han *et al*., 2004). Li *et al*. (2018) indicated that two large precipitation zones in the central part of the northern Tianshan Mountains are located at approximately 1900 and 3500 m and that precipitation decreases nonlinearly with decreasing altitude, but fluctuates according to a certain law. The results of previous studies contained significant uncertainties. The scarcity of data in high-elevation areas has been a problem to date. Most previous studies were based on rain gauge data from various sources, and thus reached different conclusions (Zhao *et al*., 2011). In this study, the CHN and

TRMM 3B43 data showed decreases above 3460 and 2870 m, respectively, indicating that there is only one zone of maximum precipitation. For the sub-regions, the CHN grid datasets generally showed monotonically increasing precipitation with increasing elevation in the northern Tianshan Mountains, except in their western and central parts (sub-regions 2 and 3). In these two sub-regions, CHN showed that precipitation decreases with increasing elevation starting at 4300 and 3700 m asl, respectively.

Figure 4 shows that for the southern Tianshan Mountains, the precipitation estimated from TRMM 3B43 increased with elevation, with a slight decrease between 4900 and 5200 m; the values ranged from 47 to 356 mm. The precipitation estimated from CHN decreased slightly above 5200 m and was higher in general than that estimated from TRMM 3B43, with values between 84 and 555 mm. Nonetheless, maxima appeared in the high-altitude (above 5200 m) region for both datasets, which is consistent with the finding of Lin (1985) that the maximum precipitation appeared above 3000 m in this region. However, other studies indicated that the precipitation first increased and then decreased with elevation, with a maximum at 2500 m (Li, 2006; Su *et al*., 2007; Chen, 2010) or approximately 3500 m (Zhou and Chen, 1998), indicating that the precipitation was lower at high altitudes than in mid-mountain regions.

In the western part (sub-region 5) of the southern Tianshan Mountains, the precipitation above 4600 m was the same as that of the entire southern Tianshan area, because these high areas appeared only in sub-region 5. For the central part (sub-region 6) of the southern Tianshan Mountains, the precipitation estimates from TRMM 3B43 increased monotonically with elevation, and the maximum appeared at the highest elevation (3900–4200 m), whereas the precipitation estimates from CHN decreased slightly above 3700 m, where the maximum precipitation appeared, as shown in Figure 4. Zhao *et al*. (2011) reported that the maximum appeared at 3332 m and that precipitation then began to decrease in sub-region 5. They also indicated that the precipitation increased monotonically with elevation and that the maximum appeared at the highest rain gauge (2458 m) in sub-region 6; however, the vertical distribution above that elevation was unclear. The precipitation profiles from CHN and TRMM 3B43 below 3332 m in sub-region 5 and below 2458 m in sub-region 6 were clearly consistent with the result of Zhao *et al*. (2011). However, the precipitation continued to increase with elevation above those elevations in this study. In the eastern part of the southern Tianshan Mountains (sub-region 7), Luo *et al*. (2000) found that the annual precipitation in the Hami region (belongs to sub-region 7) increased by 13 mm for every 100 m increase in elevation, and the annual precipitation above 4000 m asl in Yushugou Valley (which is also in sub-region 7) was 400–500 mm. Liu *et al*. (2017) reported that precipitation increased with increasing altitude from 34.5 to 1677.2 m. TRMM 3B43 data showed that precipitation first increased and then decreased slightly at 3700 m. By contrast, CHN data showed a decrease–increase–decrease pattern, with a maximum value at 2600–2900 m (Figure 4). The trend from TRMM 3B43 was similar to that reported in the above studies, but the precipitation values from TRMM 3B43 and CHN were both smaller than the reported values.

Figure 4 also shows that for the northern slopes of the Karakoram and Kunlun mountains (sub-region 8), the precipitation estimated from TRMM 3B43 first increased and then decreased with elevation; the maximum value appeared at 4800–5100 m. By contrast, the precipitation estimated from CHN increased with elevation, and the maximum value appeared

at the highest elevation. Zhao *et al*. (2011) showed that a quadratic polynomial could fit the relationship between precipitation and elevation in this region; a maximum of 106.8 mm appeared at 3840 m, which indicated that the mid-mountain region received more precipitation than higher elevations. The zone of maximum precipitation was at least 1000 m lower than the estimate from the gridded data.

Previous studies of the vertical precipitation pattern in Gansu and Inner Mongolia (sub-region 9) showed that precipitation increased nonlinearly with elevation (Zhu and Wang, 1996) or that the relationship could be described by a sigmoid curve with the maximum at the highest elevation (Tang, 1985). Chang *et al*. (2002) and Chen and Zeng (2011) found that precipitation first increased and then decreased, with maximum at 3650 m or 2600–2700 m, respectively. Sun *et al*. (2019) indicated that the maximum precipitation zones in the eastern, central, and western sections of the Qilian Mountains were 4100, 4500, and 4700 m, respectively. In this study, both gridded datasets showed that precipitation first increased and then decreased with elevation, with a maximum at 4300 m (as shown in Figure 4). This trend was consistent with the results of Chang *et al*. (2002) and Chen and Zeng (2011), and the maximum precipitation zones were similar to the result of Sun *et al*. (2019).

3.4 Limitations

The precipitation distribution in the arid region of NWC exhibits high spatiotemporal variability because of the complex topography. Topographical factors such as elevation, relative relief, slope, and aspect strongly affect the precipitation distribution. Our previous study indicated that elevation factors have the greatest effect on precipitation, followed by slope and aspect (Yang and Luo, 2014a; Yang and Luo, 2014b). In this study, the study area was divided into nine sub-regions according to the locations and aspects of the mountains, and this partition indirectly accounted for the differences between the windward and leeward sides of mountain ranges. For this reason, the elevation–precipitation relationship was analyzed, but the effects of slope and aspect were not considered in this study.

Differences in elevation over short distances can result in significant changes in the distribution of precipitation due to interactions between topography and atmospheric flow in mountainous areas (Guo *et al*., 2014). The study area has complex topography and large variation in elevation, which ranges from −154.31 to 8611 m asl. However, more than 90% of the rain gauges are located below 2000 m asl. Because of the sparsity of rain gauges in high-altitude areas, it is very difficult to derive precipitation–elevation relationships. The vertical distribution of precipitation has long been under debate. The results reported by previous studies also differed, and the precipitation–elevation profiles at high altitudes remained unclear because of the large uncertainty resulting from insufficient observations. Gridded precipitation datasets such as TRMM 3B43 and CHN cover the entire study area, including high-elevation zones, and thus the precipitation–elevation relationship can be derived. However, uncertainties remain. They may lie in the extreme sensitivity of microwave (MW) signals from clouds over complex topography and the highly variable surface in mountainous regions; the use of indirect measurement and precipitation retrieval algorithms (Rozante and Cavalcanti, 2008; Zhao and Garrett, 2008); and the misclassification of seasonal or perennial snow–ice cover as rain clouds by passive MW (Hirpa *et al*., 2010). How-

ever, these quantitative uncertainties still cannot be addressed, because very few observational data can be used for reference at high elevations.

Finally, many previous studies have analyzed precipitation frequency, intensity, and diurnal cycles using subdaily or daily datasets (Zhou *et al*., 2008; Shen *et al*., 2010; Guo *et al*., 2015; Guo *et al*., 2016). However, because of the limited temporal resolution of the corrected monthly TRMM 3B43 data, analyses at these scales could not be performed in this study.

4 Conclusions

The spatial and temporal distributions of precipitation in the arid region of NWC were analyzed using TRMM 3B43 and CHN. The results indicated annual precipitation of 137 and 143 mm over the entire study area and ranges of 53–354 mm and 78–334 mm across the nine sub-regions, respectively. TRMM 3B43 and CHN data showed that summer precipitation accounted for 36.4%–69.8% of the average annual precipitation, whereas winter precipitation accounted for only 2.5%–14%. Precipitation was more concentrated in summer in southern Xinjiang than in northern Xinjiang, and the opposite was the case in winter. Mountainous areas received more precipitation (57–204 mm) than plains (17–86 mm), especially in summer. The interannual variation of precipitation was smaller in mountainous areas than in plains, and high-altitude areas exhibited more stable annual precipitation.

Vertically, precipitation generally increased with elevation, although it may begin to decrease at certain elevations in some sub-regions. The detailed precipitation–elevation relationships in each sub-region are as follows. In the Altay Mountains, precipitation began to decrease with elevation between approximately 2560 and 3100 m and then increased again above 3100 m. For sub-regions in the northern Tianshan Mountains, precipitation increased with elevation, except in the western and central parts, according to CHN data. For the sub-regions in the southern Tianshan Mountains, precipitation increased, with slight decreases from 4900 to 5200 m (TRMM 3B43) or above 5200 m (CHN) in the western part of the Tianshan Mountains. Precipitation increased with elevation (TRMM 3B43) or decreased slightly above 3700 m (CHN) in the central part; in the eastern part, TRMM 3B43 showed that precipitation first increased and then decreased slightly at 3700 m, whereas CHN showed a decrease–increase–decrease pattern. For the northern slopes of the Karakoram and Kunlun mountains, the precipitation from CHN increased with elevation, whereas TRMM 3B43 showed an increase–decrease pattern. In Gansu and Inner Mongolia, precipitation first increased and then decreased with elevation. Overall, the maximum precipitation appeared at high altitude, and precipitation was higher there than in the corresponding mid-mountain belts.

Acknowledgments

This work was supported by National Natural Science Foundation of China (42130717). The authors thank the TRMM mission scientists and associated NASA personnel responsible for the TRMM 3B43 products and the China Meteorological Data Service Centre for providing the CHN dataset.

References

Barros A P, Chiao S, Lang T J *et al*., 2006. From weather to climate-seasonal and interannual variability of storms and implications for erosion processes in the Himalaya. *Tectonics, Climate, and Landscape Evolution*: *Geological Society of America Special Paper*, 398: 17–38.

Boushaki F I, Hsu K L, Sorooshian S *et al*., 2009. Bias adjustment of satellite precipitation estimation using ground-based measurement: A case study evaluation over the southwestern United States. *Journal of Hydrometeorology*, 10(5): 1231–1242.

Chang X X, Zhao A F, Wang J Y *et al*., 2002. Precipitation characteristic and interception of forest in Qilian Mountain. *Plateau Meteorology*, 21(3): 274–280. (in Chinese)

Chen G T, Zeng F J, 2011. Hydrological regime and water resources in the west Qilian Mountains. *Arid Zone Research*, 28(5): 744–749. (in Chinese)

Chen R S, Han C T, Liu J F *et al*., 2018. Maximum precipitation altitude on the northern flank of the Qilian Mountains, Northwest China. *Hydrological Research*, 49(5): 1696–1710.

Chen X, 2010. Physical Geography of Arid Land in China. Beijing: Science Press. (in Chinese)

Chen X, Li B L, Li Q *et al*., 2012. Spatio-temporal pattern and changes of evapotranspiration in arid central Asia and Xinjiang of China. *Journal of Arid Land*, 4(1): 105–112.

Chen X, Luo G, Xia J *et al*., 2005. Ecological response to the climate change on the northern slope of the Tianshan Mountains in Xinjiang. *Science in China Series D*: *Earth Sciences*, 48(6): 765–777.

Collischonn B, Collischonn W, Tucci C E M, 2008. Daily hydrological modeling in the Amazon basin using TRMM rainfall estimates. *Journal of Hydrology*, 360(1–4): 207–216.

De Luis M, González-Hidalgo J C, Raventós J *et al*., 1997. Distribución espacial de la concentración y agresividad de la lluvia en el territorio de la comunidad valenciana. *Cuaternarioy Geomorfologia*, 11(1): 33–44. (in Spinish)

Groisman P Y, Legates D R, 1994. The accuracy of United States precipitation data. *Bulletin of the American Meteorological Society*, 75(2): 215–227.

Guo H, Chen S, Bao A M *et al*., 2015. Comprehensive evaluation of high-resolution satellite-based precipitation products over China. *Atmosphere*, 7(1): 6.

Guo H, Chen S, Bao A M *et al*., 2016. Early assessment of integrated multi-satellite retrievals for global precipitation measurement over China. *Atmospheric Research*, 176/177: 121–133.

Guo J, Zhai P, Wu L *et al*., 2014. Diurnal variation and the influential factors of precipitation from surface and satellite measurements in Tibet. *International Journal of Climatology*, 34(9): 2940–2956.

Guo Z C, Wei W, Shi P J *et al*., 2020. Spatiotemporal changes of land desertification sensitivity in the arid region of Northwest China. *Acta Geographica Sinica*, 75(9): 1948–1965. (in Chinese)

Han T D, Ding Y J, Ye B S *et al*., 2004. Precipitation variations on the southern and northern slopes of the Tianger range in Tianshan Mountains. *Journal of Glaciology and Geocryology*, 26(6): 761–766. (in Chinese)

Hirpa F A, Gebremichael M, Hopson T, 2010. Evaluation of high-resolution satellite precipitation products over very complex terrain in Ethiopia. *Journal of Applied Meteorology and Climatology*, 49(5): 1044–1051.

Hu W F, Yao J Q, He Q *et al*., 2021. Changes in precipitation amounts and extremes across Xinjiang (northwest China) and their connection to climate indices. *Peer J*, 9(6903): e10792.

Huffman G J, Adler R F, Bolvin D T *et al*., 2007. The TRMM multi-satellite precipitation analysis (TMPA): Quasi-global, multiyear, combined-sensor precipitation estimates at fine scales. *Journal of Hydrometeorology*, 8(1): 38–55.

Huffman G J, Adler R F, Bolvin D T *et al*., 2010. The TRMM multi-satellite precipitation analysis (TMPA). In: Satellite Rainfall Applications for Surface Hydrology. Dordrecht: Springer, 3–22.

Hsu K L, Gao X G, Sorooshian S *et al*., 1997. Precipitation estimation from remotely sensed information using artificial neural networks. *Journal of Applied Meteorology and Climatology*, 36(9): 1176–1190.

Joyce R J, Janowiak J E, Arkin P A *et al*., 2004. CMORPH: A method that produces global precipitation estimates from passive microwave and infrared data at high spatial and temporal resolution. *Journal of*

Hydrometeorology, 5(3): 487–503.

Lauscher F, 1976. Weltweite typen der hohenabhangigkeit des niederschlags. *Wetter U. Leben*, 28(2): 80–90. (in Germany)

Legates D R, DeLiberty T L, 1993. Precipitation measurement biases in the United States. *JAWRA Journal of the American Water Resources Association*, 29(5): 855–861.

Li H Y, Wang K L, Jiang H *et al*., 2009. Study of the precipitation in the Heihe River basin: Progress and prospect. *Journal of Glaciology and Geocryology*, 31(2): 334–341. (in Chinese)

Li J F, 2003. Weather and Climate in the Taklamakan Desert and Surrounding Mountains. Beijing: Science Press. (in Chinese)

Li J F, 2006. The Division of Hydro-climate Resources in Urumqi River Basin. Beijing: China Meteorological Press. (in Chinese)

Li K M, Zhong X F, Jiang Y *et al*., 2018. Study on vertical gradient change of air temperature and precipitation in Urumqi River basin during 1961–2016. *Journal of Glaciology and Geocryology*, 40(3): 607–615. (in Chinese)

Lin R T, 1985. Perpendicular zonal characteristics of precipitation and runoff in the southern slope of the Tianshan Mountains. *Journal of China Hydrology*, (2): 28-33. (in Chinese)

Lin Z G, 1995. Climatology of Orographic Precipitation. Beijing: Science Press. (in Chinese)

Liu Y C, Jiao K Q, Zhao K *et al*., 2017. The response of precipitation to global climate change in the Tianshan Mountains, China. *Journal of Glaciology and Geocryology*, 39(4): 748–759. (in Chinese)

Luo G X, Ai L, Qi X M *et al*., 2002. Hydrological characteristics of the Yushugou Valley. *Desert and Oasis Meteorology*, 25(5): 19–20, 37. (in Chinese)

Luo G X, Zhang Y H, Wang Y *et al*., 2000. Analysis of contributing factors to flood caused by rainstorm and melting in Kerliker Mountain of Hami in July 1999. *Desert and Oasis Meteorology*, 23(4): 11–13. (in Chinese)

Mu Z X. 2010. Research on vertical distribution law of precipitation and snowmelt runoff simulation in high cold alpine areas [D]. Urumqi: Xinjiang Agricultural University. (in Chinese)

Ning S, Zhang Z Y, Liu L *et al*., 2020. Adaptability of precipitation estimation method based on TRMM data combined with partial least squares downscaling in different landforms of Xinjiang, China. *Transactions of the Chinese Society of Agricultural Engineering*, 36(12): 99–109. (in Chinese)

Oliver J E, 1980. Monthly precipitation distribution: A comparative index. *The Professional Geographer*, 32(3): 300–309.

Pratap S, Ramasastri K S, Naresh K, 1995. Topographical influence on precipitation distribution in different ranges of western Himalayas. *Hydrology Research*, 26(4/5): 259–284.

Qin Y H, Li B F, Chen Z S *et al*., 2018. Spatio-temporal variations of nonlinear trends of precipitation over an arid region of northwest China according to the extreme-point symmetric mode decomposition method. *International Journal of Climatology*, 38(5): 2239–2249.

Rozante J R, Cavalcanti I, 2008. Regional Eta model experiments: SALLJEX and MCS development. *Journal of Geophysical Research*: *Atmospheres*, 113: D17106.

Shen Y, Xiong A Y, Wang Y *et al*., 2010. Performance of high-resolution satellite precipitation products over China. *Journal of Geophysical Research*: *Atmospheres*, 115: D02114.

Shen Y P, Liang H, 2004. High precipitation in glacial region of high mountains in high Asia: Possible cause. *Journal of Glaciology and Geocryology*, 26(6): 806–809. (in Chinese)

Shi Y F, Shen Y P, Kang E *et al*., 2007. Recent and future climate change in northwest China. *Climatic Change*, 80(3): 379–393.

Shi Y G, Sun Z B, Yang Q, 2008. Characteristics of area precipitation in Xinjiang region with its variations. *Journal of Applied Meteorological Science*, 19(3): 326–332. (in Chinese)

Sinclair M R, Wratt D S, Henderson R D *et al*., 1997. Factors affecting the distribution and spillover of precipitation in the Southern ALPA of New Zealand: A case study. *Journal of Applied Meteorology*, 36(5): 428–442.

Su H C, Shen Y P, Han P *et al*., 2007. Precipitation and its impact on water resources and ecological environment in Xinjiang region. *Journal of Glaciology and Geocryology*, 29(3): 343–350. (in Chinese)

Sun M P, Zhang H Y, Gong N G *et al*., 2019. Study on maximum precipitation height zone in Qilian Mountains

area based on TRRM precipitation data. *Journal of Natural Resources*, 34(3): 646–657. (in Chinese)

Tang M C, 1985. The distribution of precipitation in mountain Qilian. *Acta Geographica Sinica*, 40(4): 323–332. (in Chinese)

Wang Q, Zhai P M, Qin D H, 2020. New perspectives on 'warming-wetting' trend in Xinjiang, China. *Advances in Climate Change Research*, 11(3): 252–260.

Weng D M, 1985. Analysis of the precipitation conditions in mountainous. *Meteorological Monthly*, (6): 39–43. (in Chinese)

Xie P, Gu Y Y, Zhang Y H *et al*., 2017. Precipitation and drought characteristic in Xinjiang during 1961–2015. *Arid Land Geography*, 40(2): 332–339. (in Chinese)

Xie P P, Arkin P A, 1995. An intercomparison of gauge observations and satellite estimates of monthly precipitation. *Journal of Applied Meteorology and Climatology*, 34(5): 1143–1160.

Xu M, Kang S C, Wu H *et al*., 2018. Detection of spatio-temporal variability of air temperature and precipitation based on long-term meteorological station observations over Tianshan Mountains, Central Asia. *Atmospheric Research*, 203: 141–163.

Yang Y F, Luo Y, 2014a. Evaluating the performance of remote sensing precipitation products CMORPH, PERSIANN, and TMPA, in the arid region of northwest China. *Theoretical and Applied Climatology*, 118(3): 429–445.

Yang Y F, Luo Y, 2014b. Using the back propagation neural network approach to bias correct TMPA data in the arid region of northwest China. *Journal of Hydrometeorology*, 15(1): 459–473.

Zhang J B, Deng Z F, 1987. An Outline of Xinjiang's Precipitation. Beijing: China Meteorological Press. (in Chinese)

Zhang J B, Yuan Y J, 2002. A tentative discussion on the impact of climate on surface water resources in Xinjiang. *Journal of Natural Resources*, 17(1): 28–34. (in Chinese)

Zhang K X, Su Z H, Liu J L *et al*., 2021. Characteristics of variation of precipitation concentration index and its teleconnection relationships with large-scale atmospheric circulations in Gansu Province. *Research of Soil and Water Conservation*, 28(5): 261–267. (in Chinese)

Zhang Q, Singh V P, Li J F *et al*., 2012. Spatio-temporal variations of precipitation extremes in Xinjiang, China. *Journal of Hydrology*, 434/435: 7–18.

Zhang Q, Yu Y X, Zhang J, 2008. Characteristics of water cycle in the Qilian Mountains and the oases in Hexi inland river basins. *Journal of Glaciology and Geocryology*, 30(6): 907–913. (in Chinese)

Zhang X Q, Sun Y, Zheng D *et al*., 2011. Responses of temperature zone boundaries in the arid region of China to climatic warming. *Acta Geographica Sinica*, 66(9): 1166–1178. (in Chinese)

Zhang X W, Zhang J B, 2006. Meteorological Manual in Xinjiang. Beijing: China Meteorological Press, 72–156. (in Chinese)

Zhao C, Garrett T J, 2008. Ground-based remote sensing of precipitation in the Arctic. *Journal of Geophysical Research*, 113: D14204.

Zhao C Y, Shi F Z, Sheng Y *et al*., 2011. Regional differentiation characteristics of precipitation changing with altitude in Xinjiang region in recent 50 years. *Journal of Glaciology and Geocryology*, 33(6): 1203–1213. (in Chinese)

Zhu S S, Wang Q, 1996. Temporal-spatial distributions and recent changes of precipitation in the northern slopes of the Qilian Mountains. *Journal of Glaciology and Geocryology*, 18(Suppl.1): 296–304. (in Chinese)

Zhou T J, Yu R C, Chen H M *et al*., 2008. Summer precipitation frequency, intensity, and diurnal cycle over China: A comparison of satellite data with rain gauge observations. *Journal of Climate*, 21(16): 3997–4010.

Zhou X, Chen D J, 1998. Study on vertical change features of climate in the southern slope of Tianshan Mountains. *Mountain Research*, 16(1): 47–52. (in Chinese)